Effects of Si and Mo additions on glass-forming in FeGaPCB bulk glassy alloys with high saturation magnetization

Baolong Shen,* Masahiro Akiba, and Akihisa Inoue
Institute for Materials Research, Tohoku University, Sendai 980-8577, Japan
(Received 12 September 2005; revised manuscript received 12 January 2006; published 20 March 2006)

We investigated the effect of Si and Mo additions on the glass-forming ability (GFA) of Fe-Mo-Ga-P-C-B-Si alloys. The simultaneous addition of small amounts of Si and Mo was found to be effective for extension of the supercooled liquid region (ΔT_x) defined by the difference between glass transition temperature (T_g) and crystallization temperature (T_x). The ΔT_x value is 26 K for the $Fe_{78}Ga_2P_{12}C_4B_4$ glassy alloy, and increases to 52 and 50 K for the $Fe_{76}Mo_2Ga_2P_{10}C_4B_4Si_2$ and $Fe_{74}Mo_4Ga_2P_{10}C_4B_4Si_2$ glassy alloys, respectively. Similarly, the ΔT_x value is 33 K for the $Fe_{77}Ga_3P_{12}C_4B_4$ glassy alloy, and increases to 60 and 57 K for the $Fe_{75}Mo_2Ga_3P_{10}C_4B_4Si_2$ and $Fe_{73}Mo_4Ga_3P_{10}C_4B_4Si_2$ glassy alloys, respectively. These four glassy alloys also exhibit rather high reduced glass transition temperature (T_g/T_l) of 0.58–0.60. By copper mold casting, bulk glassy alloy rods with the diameters of 1.5 to 2.5 mm were prepared. These four glassy alloys also exhibit high saturation magnetization (I_s) of 1.11–1.32 T and good soft-magnetic properties, i.e., low coercive force (H_c) of 2.4–3.3 A/m, and high effective permeability (μ_e) at 1 kHz of 8500–14 000. The relation between crystallization behavior and GFA was also investigated. It was found that the primary precipitation phase of the Fe-Mo-Ga-P-C-B-Si glassy alloys is a complex fcc $(Fe,Mo)_{23}(B,C)_6$ phase, and the addition of small amounts of Si and Mo is effective for the suppression of precipitation of $(Fe,Mo)_{23}(B,C)_6$ phase, resulting in the extension of ΔT_x and the improvement of GFA.

DOI: 10.1103/PhysRevB.73.104204 PACS number(s): 64.70.Pf, 75.50.Kj, 81.05.Kf

I. INTRODUCTION

Beginning in 1988, bulk glassy alloys (BGAs) consisting only of metallic components in Mg- and lanthanide (Ln)-based systems were synthesized by copper mold casting for the first time.[1,2] From then, a large number of BGAs have been developed and some BGAs have been used as engineering materials.[3] In the case of Fe-based BGAs, since the first finding of glass transition before crystallization in Fe-based amorphous alloys, followed by synthesis of Fe-(Al, Ga)-(P,C,B) BGAs,[4,5] a large number of Fe-based ferromagnetic BGAs have been developed as soft magnetic materials.[6,7] Now, the development of Fe-based BGAs with high glass-forming ability (GFA) has attracted increasing interest of high potential for applications as structural[8–11] and functional (ferromagnetic)[12–17] materials. However, for the ferromagnetic BGAs, the development always includes a discrepancy between GFA and saturation magnetization (I_s), because the addition of glass-forming elements decreases Fe content, resulting in the decrease of I_s. Consequently, many Fe-based ferromagnetic BGAs with a large supercooled liquid region (ΔT_x) before crystallization exhibit low I_s below 1 T,[6,12–14,17] and the increase of I_s has strongly been requested for the extension of application fields as soft-magnetic materials.

Recently, we developed $Fe_{65}Co_{10}Ga_5P_{12}C_4B_4$ and $Fe_{77}Ga_3P_{9.5}C_4B_4Si_{2.5}$ BGAs exhibiting 1.2 and 1.37 T, respectively, for I_s, and 50 and 45 K, respectively, for ΔT_x.[18,19] The large ΔT_x values enabled us to synthesize Fe-based BGAs with diameters up to 20 mm by the consolidation method utilizing viscous flowability in the supercooled liquid state.[20,21] However, the size is not large enough to apply to the magnetic cores used for motor engines. Ferromagnetic Fe-based BGAs with large ΔT_x, which is needed for the suppression of crystallization by the powder sintering process, have been searched for, and a Fe-Mo-Ga-P-C-B-Si BGA containing 3 at. % Ga has been synthesized.[22] However, there has been a strong demand to reduce materials cost through a decrease in Ga content. Fe-based BGAs with lower Ga content of 2 at. % were also synthesized by adding Si and Mo additions. This paper presents in detail the formation and properties of Fe-based BGAs Fe-Mo-Ga-P-C-B-Si with 2 and 3 at. % Ga contents. The effects of additional Si and Mo elements on the thermal stability of the supercooled liquid as well as the relation between crystallization behavior and GFA are also investigated.

II. EXPERIMENT

Multicomponent alloy ingots with compositions of $Fe_{78}Ga_2P_{12-x}C_4B_4Si_x$, $Fe_{78-x}Mo_xGa_2P_{10}C_4B_4Si_2$, and $Fe_{77-x}Mo_xGa_3P_{10}C_4B_4Si_2$ were prepared by induction melting. Their compositions are nominally expressed in atomic percentage. As it has been confirmed that scavenging oxygen impurities is effective in improving the GFA,[10] the alloy ingots were prepared under a high purified argon atmosphere by using the elements with high purity of Fe (99.9 ms. %), Mo (99.9 ms. %), Ga (99.9999 ms. %), B (99.9 ms. %) and Si (99.99 ms. %) in this study. P and C were alloyed by adding pre-alloyed Fe-26.5 ms. %P and Fe-4.1 ms. %C ingots, which were also prepared by induction melting, and exhibited high purities of 99.9 ms. %, respectively. Before induction melting, the chamber of the induction furnace was first evacuated to 10^{-3} Pa by a diffusion pump, and then flushed three times with high purified argon gas

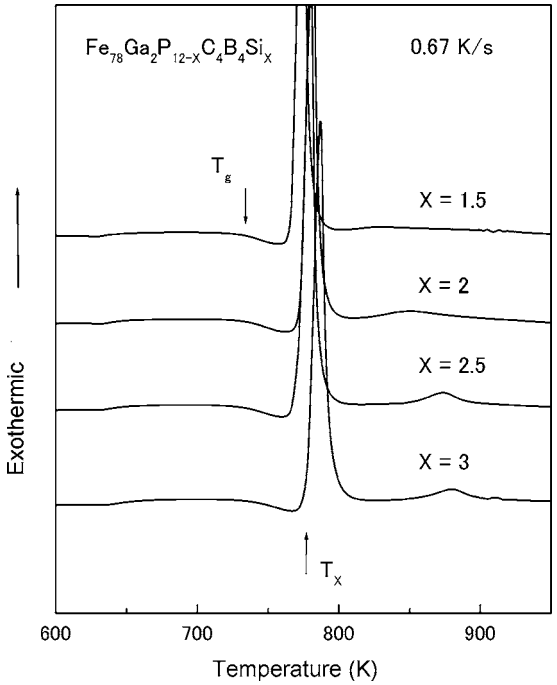

FIG. 1. DSC curves of melt-spun $Fe_{78}Ga_2P_{12-x}C_4B_4Si_x$ (x=1.5, 2, 2.5 and 3) glassy alloys.

(99.99 ms. %) for obtaining the high purified argon atmosphere. From the master alloy ingots, glassy alloy ribbons with a cross section of 0.02×1 mm^2 were prepared by melt spinning. Cylindrical rods with diameters up to 3 mm and a length of 40 mm were prepared by injecting the molten alloys contained in a quartz tube into the cylinder-shaped cavity of a copper mold under a high purified argon atmosphere, which is the same as that when preparing alloy ingots. The glassy and crystallized structures were identified by x-ray diffraction (XRD) with Cu $K\alpha$ radiation. The glassy alloy rods in as-cast and annealed states were sectioned by a fine cutter for XRD measurement. The absence of micrometer scale crystalline phase was also examined by optical microscopy. Thermal stability associated with glass transition temperature (T_g), crystallization temperature (T_x), and ΔT_x was examined by differential scanning calorimetry at a heating rate of 0.67 K/s. Liquidus temperature (T_l) was measured by cooling the alloy melt with a differential thermal analyzer (DTA). To reduce influence of undercooling, DTA measurement was performed at a low cooling rate of 0.067 K/s. Magnetic properties of I_s, coercive force (H_c), and effective permeability (μ_e) at 1 kHz were measured with a vibrating sample magnetometer under an applied field of 400 kA/m, a B-H loop tracer under a field of 800 A/m, and an impedance analyzer under a field of 1 A/m, respectively.

III. RESULTS

Figure 1 shows DSC curves of the melt-spun $Fe_{78}Ga_2P_{12-x}C_4B_4Si_x$ (x=1.5, 2, 2.5, and 3) glassy alloys. The largest ΔT_x of 41 K was obtained for $Fe_{78}Ga_2P_{10}C_4B_4Si_2$ glassy alloy. The further increase in Si content resulted in an obvious two-stage crystallization, accompanying a decrease in ΔT_x. Therefore, an optimum content of Si is determined as 2 at. %.

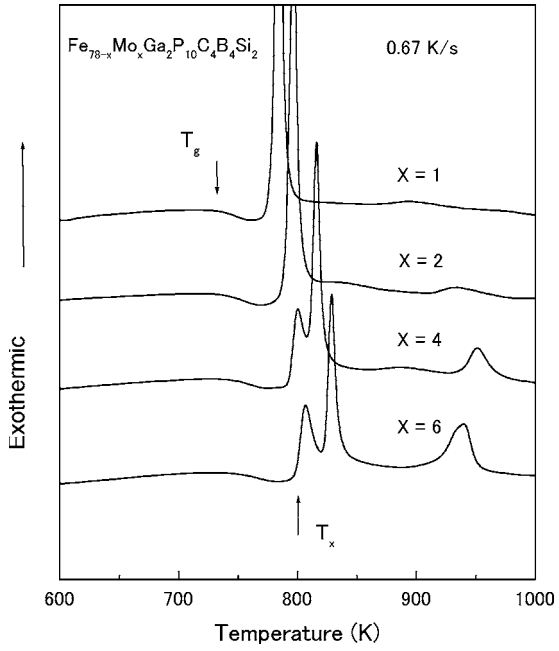

FIG. 2. DSC curves of melt-spun $Fe_{78-x}Mo_xGa_2P_{10}C_4B_4Si_2$ (x =1, 2, 4, and 6) glassy alloys.

Figures 2 and 3 show DSC curves of the melt-spun $Fe_{78-x}Mo_xGa_2P_{10}C_4B_4Si_2$ (x=1, 2, 4, and 6) and $Fe_{77-x}Mo_xGa_3P_{10}C_4B_4Si_2$ (x=1, 2, 4, and 6) glassy alloys, respectively. It is seen that all alloys exhibit glass transition, followed by a supercooled liquid region and then crystallization. As the Mo content increases from 1 to 2 at. %, the ΔT_x increases from 43 to 52 K for the $Fe_{78-x}Mo_xGa_2P_{10}C_4B_4Si_2$ glassy alloys, and from 44 to 60 K for the

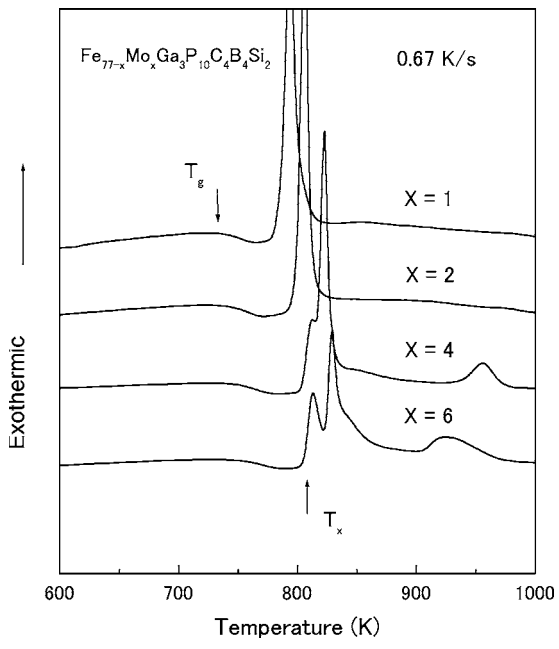

FIG. 3. DSC curves of melt-spun $Fe_{77-x}Mo_xGa_3P_{10}C_4B_4Si_2$ (x =1, 2, 4, and 6) glassy alloys.

$Fe_{77-x}Mo_xGa_3P_{10}C_4B_4Si_2$ glassy alloys. The ΔT_x values are larger than those (26–33 K) for the $Fe_{78}Ga_2P_{12}C_4B_4$ and $Fe_{77}Ga_3P_{12}C_4B_4$ glassy alloys.[23] Thus, the simultaneous addition of small amounts of Si and Mo elements is effective for the extension of the supercooled liquid region. It is also seen that the crystallization for both the two glassy alloy systems takes place through a single exothermic stage when Mo content is below 2 at. %. The further increase in Mo content caused a three-stage crystallization, accompanying a decrease in ΔT_x. This means that the precipitation of the crystalline phases for both the 2 at. %Mo-containing glassy alloys is more difficult, and their supercooled liquids are more stable than those of the other glassy alloys. Thus, the $Fe_{76}Mo_2Ga_2P_{10}C_4B_4Si_2$ and $Fe_{75}Mo_2Ga_3P_{10}C_4B_4Si_2$ glassy alloys have the internal equilibrium state with fully relaxed glassy structure in the temperature intervals of 17 and 22 K, respectively, before crystallization during continuous heating at a rate of 0.67 K/s. The stable supercooled liquid is important for the utilization of viscous flowability by the powder sintering process.[20,21,24] We also measured T_l by DTA with the aim at determining the reduced glass transition temperature (T_g/T_l), which has been regarded as one of the important parameters for evaluating GFA.[3] The T_g/T_l value is 0.59 for $Fe_{76}Mo_2Ga_2P_{10}C_4B_4Si_2$ and 0.60 for $Fe_{75}Mo_2Ga_3P_{10}C_4B_4Si_2$, suggesting that higher GFA is obtained for these 2 at. % Mo-containing glassy alloys.

Consequently, we tried to form cylindrical glassy alloy rods and their critical diameters were determined to be 1.5 mm for $Fe_{74}Mo_4Ga_2P_{10}C_4B_4Si_2$, 2 mm for $Fe_{76}Mo_2Ga_2P_{10}C_4B_4Si_2$, 2 mm for $Fe_{73}Mo_4Ga_3P_{10}C_4B_4Si_2$, and 2.5 mm for $Fe_{75}Mo_2Ga_3P_{10}C_4B_4Si_2$. As examples, Fig. 4 shows XRD patterns of the cast $Fe_{76}Mo_2Ga_2P_{10}C_4B_4Si_2$ rod with a diameter of 2 mm and the $Fe_{75}Mo_2Ga_3P_{10}C_4B_4Si_2$ rods with diameters of 2 and 2.5 mm, together with their XRD patterns of the melt-spun glassy alloy ribbon with a thickness of 20 μm, respectively. Only a broad peak is seen around a diffraction angle of 44° for these bulk samples, indicating the formation of a glassy phase. We have also confirmed the formation of BGAs without micrometer scale crystalline phase by optical microscopy. The thermal stability of the BGAs was also examined by DSC. Figure 5 shows DSC curves of the $Fe_{76}Mo_2Ga_2P_{10}C_4B_4Si_2$ glassy rod with a diameter of 2 mm and the $Fe_{75}Mo_2Ga_3P_{10}C_4B_4Si_2$ glassy rods with diameters of 2 and 2.5 mm. The DSC curves of the melt-spun glassy alloy ribbons are also shown for comparison. No appreciable difference in ΔT_x and crystallization process is recognized between the melt-spun ribbons and the BGAs, indicating the formation of the similar glassy phase, although the T_g and T_x of the BGAs shifted slightly to the high-temperature side for the $Fe_{75}Mo_2Ga_3P_{10}C_4B_4Si_2$ glassy alloy presumably because of the uses of different ingots for preparing ribbon and bulk samples. Therefore, it is concluded that the $Fe_{76}Mo_2Ga_2P_{10}C_4B_4Si_2$ and $Fe_{75}Mo_2Ga_3P_{10}C_4B_4Si_2$ glassy alloys exhibit the highest GFA in each alloy system, and the simultaneous addition of 2 at. % Si and 2 at. %Mo is very effective for improving the GFA of Fe-Ga-(P,C,B) alloys.

Magnetic properties of these two glassy alloy systems were also measured. With an increase of Mo content, I_s of the $Fe_{78-x}Mo_xGa_2P_{10}C_4B_4Si_2$ (x=1, 2, 4, and 6) and

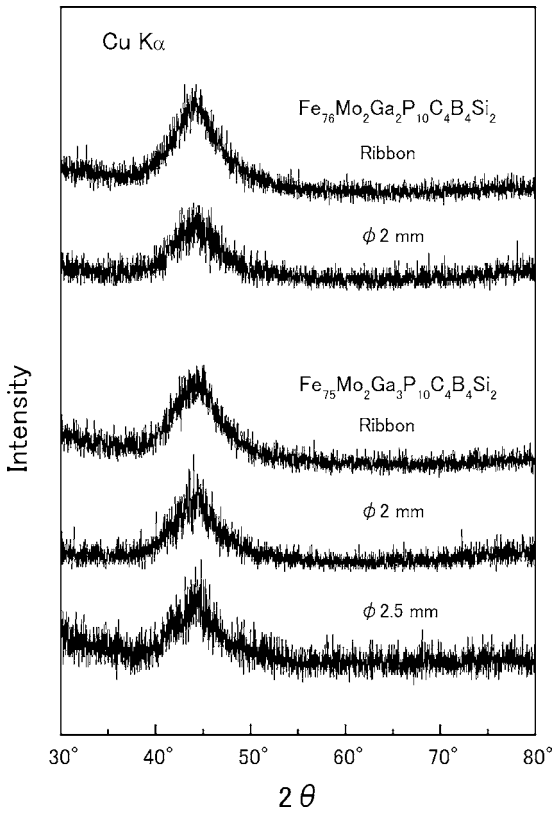

FIG. 4. XRD patterns of the cast $Fe_{76}Mo_2Ga_2P_{10}C_4B_4Si_2$ rod with a diameter of 2 mm and $Fe_{75}Mo_2Ga_3P_{10}C_4B_4Si_2$ rods with diameters of 2 and 2.5 mm, together with the XRD patterns of the melt-spun glassy alloy ribbons with a thickness of 20 μm.

$Fe_{77-x}Mo_xGa_3P_{10}C_4B_4Si_2$ (x=1, 2, 4, and 6) glassy alloys decreases from 1.41 to 1.05 T, and 1.36 to 0.98 T, respectively, because of the decrease of Fe content. The H_c of the two series of glassy alloys measured with a *B-H* loop tracer is in the range from 2 to 4 A/m, and the μ_e at 1 kHz lies between 7100 and 14 000.

Table I summarizes the maximum diameter (D_{max}), thermal stability and magnetic properties of the $Fe_{78-x}Mo_xGa_2P_{10}C_4B_4Si_2$ and $Fe_{77-x}Mo_xGa_3P_{10}C_4B_4Si_2$ (x =2 and 4) BGAs. It is seen from the table that the soft-magnetic properties change in proportion to the GFA. The $Fe_{76}Mo_2Ga_2P_{10}C_4B_4Si_2$ and $Fe_{75}Mo_2Ga_3P_{10}C_4B_4Si_2$ glassy alloys with the highest GFA in each alloy system exhibit the best soft-magnetic properties. The reason can be interpreted to result from the formation of a glassy structure with a high level of homogeneity in the absence of any crystalline nuclei.[25] The values of D_{max}, ΔT_x, I_s, H_c, and μ_e at 1 kHz are 2 mm, 52 K, 1.32 T, 2.9 A/m and 9700, respectively, for the former alloy, and 2.5 mm, 60 K, 1.27 T, 2.4 A/m and 14 000, respectively, for the latter alloy. Thus, Fe-based BGAs with high I_s of over 1.25 T, large ΔT_x of over 50 K and high GFA of over 2 mm in diameter have been synthesized.

IV. DISCUSSION

As described above, the simultaneous addition with small amounts of Si and Mo to the $Fe_{78}Ga_2P_{12}C_4B_4$ and

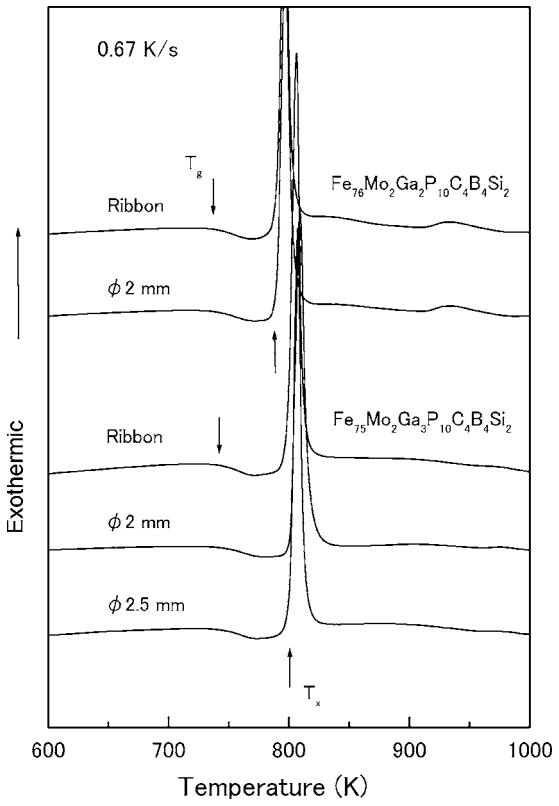

FIG. 5. DSC curves of the $Fe_{76}Mo_2Ga_2P_{10}C_4B_4Si_2$ glassy rod with a diameter of 2 mm and $Fe_{75}Mo_2Ga_3P_{10}C_4B_4Si_2$ glassy rods with diameters of 2 and 2.5 mm. The DSC curves of the melt-spun glassy alloy ribbons are also shown for comparison.

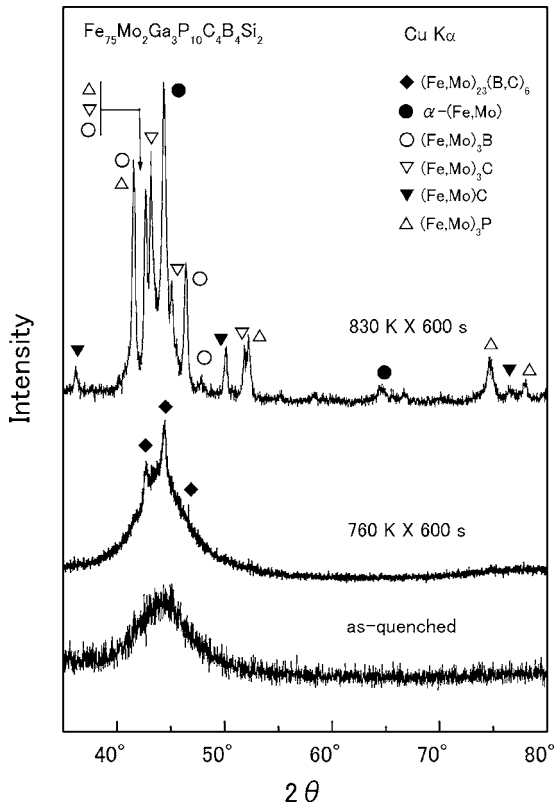

FIG. 6. XRD patterns of the $Fe_{75}Mo_2Ga_3P_{10}C_4B_4Si_2$ glassy alloy subjected to annealing for 600 s at temperatures of 760 and 830 K. The XRD pattern of the as-quenched alloy is also shown for comparison.

$Fe_{77}Ga_3P_{12}C_4B_4$ glassy alloys leads to the significant extension of the supercooled liquid region as well as the significant increase of the GFA. Figures 2 and 3 show that the extension of ΔT_x is attributed to the retardation of crystallization. To exhaust the reason why the crystallization was suppressed for the 2 at. %Mo-containing glassy alloys, the crystallization behavior was investigated. Figure 6 shows XRD patterns of the $Fe_{75}Mo_2Ga_3P_{10}C_4B_4Si_2$ glassy alloy subjected to annealing for 600 s at the temperatures of 760 and 830 K, corresponding to the temperatures just below and above the exothermic peak in the DSC curve. The XRD pattern of the as-quenched alloy with a glassy structure is also shown for comparison. As shown in Fig. 6, the XRD patterns of the sample annealed at 760 K are identified as a single face-centered cubic $(Fe,Mo)_{23}(B,C)_6$ phase with a large lattice parameter of over 1 nm including 96 atoms,[26] and as mixed α-(Fe,Mo), $(Fe,Mo)_3B$, $(Fe,Mo)_3C$, (Fe,Mo)C, and $(Fe,Mo)_3P$ phases for the sample annealed at 830 K corresponding to the temperature above the exothermic peak. The primary precipitation phase of $(Fe,Mo)_{23}(B,C)_6$ is in a metastable state, being consistent with the results obtained from Fe-B-Si-based BGAs.[27] Consequently, it is considered that the Fe-P-C-based BGAs also behave a unique network-like structure, which leads to the high stability of the supercooled liquid against crystallization.[28] The same results were also obtained by Ponnambalam *et al.* from Fe-Mn-Cr-Mo-C-B BGAs that metastable $Fe_{23}C_6$ phase is indeed the primary phase which competes with the formation of the glassy phase, and the $Fe_{23}C_6$ phase that forms as a single devitrified phase at T_x of 873 K is found to decompose into several

TABLE I. Maximum diameter, thermal stability and magnetic properties of $Fe_{78-x}Mo_xGa_2P_{10}C_4B_4Si_2$ and $Fe_{77-x}Mo_xGa_3P_{10}C_4B_4Si_2$ (x=2 and 4) glassy alloys rods.

	Diameter	Thermal stability			Magnetic properties		
Alloy	D_{max} (mm)	T_g (K)	ΔT_x (K)	T_g/T_1	I_s (T)	H_c(Am^{-1})	μ_e(1 kHz)
$Fe_{76}Mo_2Ga_2P_{10}C_4B_4Si_2$	2	736	52	0.59	1.32	2.9	9 700
$Fe_{74}Mo_4Ga_2P_{10}C_4B_4Si_2$	1.5	740	50	0.58	1.16	3.3	8 500
$Fe_{75}Mo_2Ga_3P_{10}C_4B_4Si_2$	2.5	738	60	0.60	1.27	2.4	14 000
$Fe_{73}Mo_4Ga_3P_{10}C_4B_4Si_2$	2	744	57	0.58	1.11	3.0	11 500

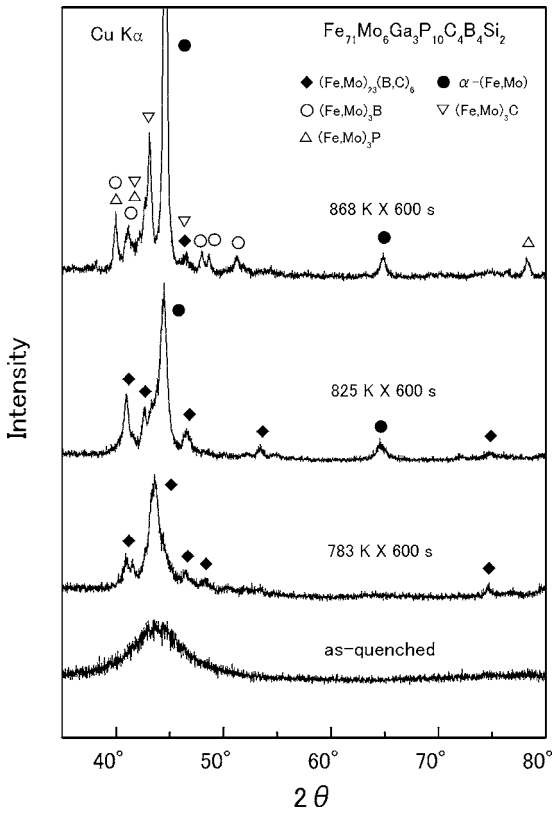

FIG. 7. XRD patterns of the $Fe_{71}Mo_6Ga_3P_{10}C_4B_4Si_2$ glassy alloy subjected to annealing for 600 s at temperatures of 783, 825, and 868 K. The XRD pattern of the as-quenched alloy is also shown for comparison.

other phases after being annealed at 973 K.[29] In this study, it is considered that the formation of the metastable $(Fe,Mo)_{23}(B,C)_6$ phase upon the devitrification of Fe-Mo-Ga-P-C-B-Si is drastically impeded[9] by alloying with small amounts of Si and Mo, because the mixing enthalpies with large negative values between Si and Fe or Mo[30] could increase the difficulty of the formation of the metastable $(Fe,Mo)_{23}(B,C)_6$ phase. In addition, the large (Fe and Mo) and small (B and C) atoms[31] may form a reinforced "backbone" in the amorphous structure, which would also suppress the crystallization.[32] These two effects increase the stability of the undercooled melt, resulting in the enhancement of the GFA.

On the other hand, as also shown in Figs. 2 and 3, respectively, the 6 at. % Mo-containing glassy alloy exhibits the most distinguished three-stage crystallization behavior in both alloy systems. Here, the crystallization behavior was also investigated. Figure 7 shows XRD patterns of the $Fe_{71}Mo_6Ga_3P_{10}C_4B_4Si_2$ glassy alloy subjected to annealing for 600 s at the temperatures of 783 and 825 K corresponding to the temperatures just below and above the first exothermic peak, as well as at the temperature of 868 K corresponding to the temperature above the second exothermic peak. The primary precipitation phase of the $Fe_{71}Mo_6Ga_3P_{10}C_4B_4Si_2$ glassy alloy is also the $(Fe,Mo)_{23}(B,C)_6$ phase. The crystallization phase of the sample annealed at the temperature of 825 K were $(Fe,Mo)_{23}(B,C)_6$ and α-(Fe,Mo) phases, and the XRD patterns of the sample annealed at 868 K corresponding to the temperature above the second peak were identified as the mixed phases of $(Fe,Mo)_{23}(B,C)_6$, $(Fe,Mo)_3C$, α-(Fe,Mo), $(Fe,Mo)_3B$, and $(Fe,Mo)_3P$. As the first and the second peaks overlap each other at the temperature of 825 K, it is considered that the first exothermic peak is attributed to the precipitation of the $(Fe,Mo)_{23}(B,C)_6$ phase, which causes the decrease of ΔT_x. Consequently, as mentioned above, the supercooled liquid of the 2 at. %Mo-containing alloy is in the most stable state because precipitation of the $(Fe,Mo)_{23}(B,C)_6$ phase was suppressed, and the supercooled liquid becomes unstable against crystallization with increasing Mo content to over 2 at. %. Otherwise, from the XRD patterns of the $Fe_{75}Mo_2Ga_3P_{10}C_4B_4Si_2$ and $Fe_{71}Mo_6Ga_3P_{10}C_4B_4Si_2$ glassy alloys annealed at the temperatures of 760 and 783 K as shown in Figs. 6 and 7, it can be seen that the diffraction peaks of the $(Fe,Mo)_{23}(B,C)_6$ phase in the latter alloy are much stronger than those of the $(Fe,Mo)_{23}(B,C)_6$ phase in the former alloy, suggesting that the stability of the $(Fe,Mo)_{23}(B,C)_6$ phase relative to the amorphous structure increased in the $Fe_{71}Mo_6Ga_3P_{10}C_4B_4Si_2$ glassy alloy.[29] As a result, the precipitation of the $(Fe,Mo)_{23}(B,C)_6$ phase of the $Fe_{71}Mo_6Ga_3P_{10}C_4B_4Si_2$ glassy alloy is more easier than that of the $Fe_{75}Mo_2Ga_3P_{10}C_4B_4Si_2$ glassy alloy, resulting in the decrease of stability of the supercooled liquid. Thus, the preparation of BGAs becomes difficult for the 6 at. %Mo-containing alloy. The reason may be considered to result from the negative mixing enthalpy with a value of 19 kJ/mol between Mo and B,[33] which increases the bonding nature of Mo-B atomic pair as the Mo content increases to over 4 at. %, and therefore, resulting in the increase of the stability of the $(Fe,Mo)_{23}(B,C)_6$ phase relative to the amorphous structure. In addition, it is also recognized that the ΔT_x increases with increasing Ga content, being consistent with the former result.[23]

V. CONCLUSIONS

With the aim of exploring Fe-based glassy alloys with large ΔT_x, high GFA and high I_s, we examined the effects of Si and Mo additions on the ΔT_x, GFA, and I_s of the $Fe_{78-x}Mo_xGa_2P_{10}C_4B_4Si_2$ and $Fe_{77-x}Mo_xGa_3P_{10}C_4B_4Si_2$ glassy alloys. The results obtained are summarized as follows.

(1) The small amounts of Si and Mo additions are effective for the extension of ΔT_x and improvement of GFA. By simultaneously adding 2 at. % Si as well as 2 to 4 at. %Mo, the $Fe_{78-x}Mo_xGa_2P_{10}C_4B_4Si_2$ and $Fe_{77-x}Mo_xGa_3P_{10}C_4B_4Si_2$ ($x=2$ and 4) glassy alloys exhibit large ΔT_x of 50–60 K and high T_g/T_l of 0.58–0.60.

(2) The extension of ΔT_x is attributed to the existence of the unique network-like structure in the supercooled liquid and the suppression of precipitation of $(Fe,Mo)_{23}(B,C)_6$ phase caused by the small amounts of additions of Si and Mo. The stable supercooled liquid as well as high T_g/T_l leads to the synthesis of BGAs with diameters of 1.5–2.5 mm for

the $Fe_{78-x}Mo_xGa_2P_{10}C_4B_4Si_2$ and $Fe_{77-x}Mo_xGa_3P_{10}C_4B_4Si_2$ ($x=2$ and 4) glassy alloys by copper mold casting.

(3) The $Fe_{78-x}Mo_xGa_2P_{10}C_4B_4Si_2$ and $Fe_{77-x}Mo_xGa_3P_{10}C_4B_4Si_2$ ($x=2$ and 4) glassy alloys exhibit high I_s of 1.11–1.32 T, and good soft-magnetic properties; i.e., low H_c of 2.4–3.3 A/m, and high μ_e at 1 kHz of 8500–14 000. The combination of large supercooled liquid region and high glass-forming ability as well as high saturation magnetization and good soft-magnetic properties allows us to expect that the Fe-based bulk glassy alloys find application fields as new functional materials.

ACKNOWLEDGMENTS

This work was supported by Research and Development Project, SORST, Japan Science and Technology Agency (JST).

*Author to whom correspondence should be addressed. Electronic address: shen@imr.tohoku.ac.jp

[1] A. Inoue, K. Ohtera, K. Kita, and T. Masumoto, Jpn. J. Appl. Phys., Part 2 **27**, L2248 (1988).
[2] A. Inoue, T. Zhang, and T. Mosumoto, Mater. Trans., JIM **30**, 965 (1989).
[3] A. Inoue, Acta Mater. **48**, 279 (2000).
[4] A. Inoue and J. S. Gook, Mater. Trans., JIM **36**, 1180 (1995).
[5] A. Inoue, Y. Shinohara, and J. S. Gook, Mater. Trans., JIM **36**, 1427 (1995).
[6] T. D. Shen and R. B. Schwarz, Appl. Phys. Lett. **75**, 49 (1999).
[7] A. Inoue, A. Takeuchi, and B. L. Shen, Mater. Trans., JIM **42**, 970 (2001).
[8] V. Ponnambalam, S. J. Poon, G. J. Shiflet, V. M. Keppens, R. Taylor, and G. Petculescu, Appl. Phys. Lett. **83**, 1131 (2003).
[9] V. Ponnambalam, S. J. Poon, and G. J. Shiflet, J. Mater. Res. **19**, 1320 (2004).
[10] Z. P. Lu, C. T. Liu, and W. D. Porter, Appl. Phys. Lett. **83**, 2581 (2003).
[11] Z. P. Lu, C. T. Liu, J. R. Thompson, and W. D. Porter, Phys. Rev. Lett. **92**, 245503 (2004).
[12] P. Pawlik, H. A. Davies, and M. R. J. Gibbs, Appl. Phys. Lett. **83**, 2775 (2003).
[13] W. H. Wang, M. X. Pan, D. Q. Zhao, Y. Hu, and H. Y. Bai, J. Phys.: Condens. Matter **16**, 3719 (2004).
[14] R. B. Schwarz, T. D. Shen, U. Harms, and T. Lillo, J. Magn. Magn. Mater. **283**, 223 (2004).
[15] K. Amiya, A. Urata, N. Nishiyama, and A. Inoue, Mater. Trans., JIM **45**, 1214 (2004).
[16] B. L. Shen, A. Inoue, and C. T. Chang, Appl. Phys. Lett. **85**, 4911 (2004).
[17] M. Stoica, S. Roth, J. Eckert, L. Schultz, and M. D. Baro, J. Magn. Magn. Mater. **290-291**, 1480 (2005).
[18] B. L. Shen, H. M. Kimura, A. Inoue, and T. Mizushima, Mater. Trans., JIM **41**, 1675 (2000).
[19] B. L. Shen and A. Inoue, Mater. Trans., JIM **43**, 1235 (2002).
[20] B. L. Shen and A. Inoue, J. Mater. Res. **18**, 2115 (2003).
[21] B. L. Shen, H. M. Kimura, and A. Inoue, Mater. Sci. Forum **475-479**, 3397 (2005).
[22] M. Akiba, B. L. Shen, and A. Inoue, Mater. Trans., JIM **46**, 2773 (2005).
[23] B. L. Shen and A. Inoue, J. Mater. Sci. Lett. **22**, 857 (2003).
[24] Y. Kawamura, H. Kato, A. Inoue, and T. Masumoto, Appl. Phys. Lett. **67**, 2008 (1995).
[25] A. Inoue, Mater. Sci. Eng., A **304-306**, 1 (2001).
[26] M. Imafuku, S. Sato, H. Koshiba, E. Matsubara, and A. Inoue, Mater. Trans., JIM **41**, 1526, (2000).
[27] A. Inoue and B. L. Shen, Adv. Mater. (Weinheim, Ger.) **16**, 2189 (2004).
[28] E. Matsubara, S. Sato, M. Imafuku, T. Nakamura, H. Koshiba, A. Inoue, and Y. Waseda, Mater. Sci. Eng., A **312**, 136 (2001).
[29] V. Ponnambalam, S. J. Poon, and G. J. Shiflet, J. Mater. Res. **19**, 3046 (2004).
[30] F. R. De Boer, R. Boom, W. C. M. Mattens, A. R. Miedema, and A. K. Niessen, in *Cohesion in Metals*, edited by F. R. De Boer and D. G. Pettifor (North-Holland, Amsterdam, 1989), p. 217.
[31] *Metals Databook* (The Japan Institute of Metals, Maruzan, Tokyo, 2004), p. 8.
[32] S. J. Poon, G. J. Shiflet, F. Q. Guo, and V. Ponnambalam, J. Non-Cryst. Solids **317**, 1 (2003).
[33] F. R. De Boer, R. Boom, W. C. M. Mattens, A. R. Miedema, and A. K. Niessen, in *Cohesion in Metals*, edited by F. R. De Boer and D. G. Pettifor (North-Holland, Amsterdam, 1989), p. 403.